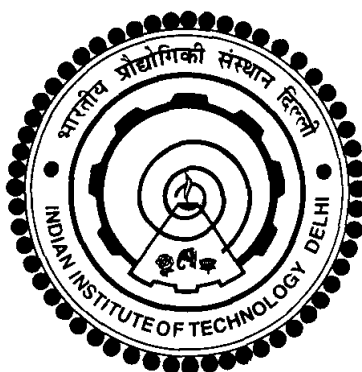


NANOSTRUCTURED ALLOYS FOR ELECTROCATALYSIS

SOUMEN SAHA



**DEPARTMENT OF CHEMISTRY
INDIAN INSTITUTE OF TECHNOLOGY DELHI
OCTOBER 2017**

©Indian Institute of Technology Delhi (IITD), New Delhi, 2017

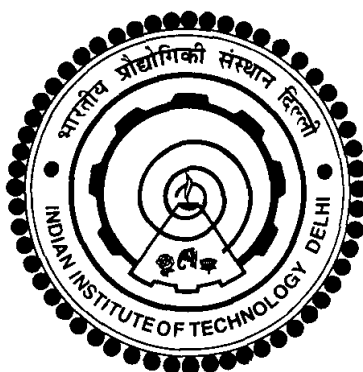
NANOSTRUCTURED ALLOYS FOR ELECTROCATALYSIS

by

SOUMEN SAHA
Department of Chemistry

Submitted
in fulfillment of the requirements of the degree of Doctor of Philosophy

to the



INDIAN INSTITUTE OF TECHNOLOGY DELHI

OCTOBER 2017

*Dedicated to
My Parents and My Wife*

CERTIFICATE

This is to certify that the thesis entitled, “**NANOSTRUCTURED ALLOYS FOR ELECTROCATALYSIS**”, being submitted by **Mr. Soumen Saha** to the Indian Institute of Technology, Delhi for the award of the degree of **Doctor of Philosophy** in Chemistry, is a record of bonafide research work carried out by him. Mr. Soumen Saha has worked under our guidance and supervision, and has fulfilled the requirements for the submission of this thesis, which to our knowledge has reached the requisite standard.

The results contained in this dissertation have not been submitted in part or full, to any other university or institute for award of any degree or diploma.

Date:

Dr. Sonalika Vaidya
Scientist C
Institute of Nano Science
& Technology
Habitat Centre, Sector-64,
Phase X, Mohali
Lien on from: Department of Chemistry
Hindu College

Prof. Ashok K Ganguli
Professor
Department of Chemistry
Indian Institute of Technology, Delhi
New Delhi-110016, India

ACKNOWLEDGMENTS

First of all, I would like to extend my deepest sincere gratitude to my PhD supervisor, Professor Ashok K Ganguli, Director, Institute of Nano Science and Technology, Mohali, and Professor at Department of Chemistry, IIT Delhi for his valuable guidance, helpful discussions and support throughout the journey. His precious advices, suggestions and encouragement throughout this work leading me on the way toward a scientific researcher.

I am grateful to Dr. Pramit Chowdhury for his help, suggestions and cooperation in absence of my research supervisor. I am also thankful to the former head Prof. A. K. Singh and present head Prof. Ravi Shankar of Department of Chemistry for providing me all necessary facilities in the department

I am also very thankful to my SRC (Student Research Committee) members, Prof. S. Basu (external committee member), Prof. A. Ramanan (former Head) and Dr. S. Deep for their comments, information and suggestions over the past years.

I also thank to INST Mohali and NRF IIT Delhi for providing me the all necessary facilities.

The thanks also go to Professor Ramanujachary and Professor Samuel Rowan University, U.S.A. who helped me in magnetic measurements of my samples. I also want to thank Dr. Pravin Ingole to allow me to carry out the electrochemical measurements in his laboratory and helped me so much by providing his valuable advices and suggestions. I also want to thank Prof. Shivaprasad (JNCASR) for XPS measurements.

I am also grateful to my lab-colleagues, past and current group members, Dr. Sonalika, Dr. Aparna, Dr. Masood Nath, Dr. Jai Prakash, Dr. Jahangeer, Dr. Menaka, Dr. Mrinmoyee, Dr. Sharmila, Dr. R. Parthasarathy, Dr. Soma, Dr. Manu Sharma, Dr. Anjaniyulu, Dr. Debashree,

Dr. Sunita, Dr. Neha, Dr. Sharmila, Nibedita, Zeba, Nitin, Vaishali, Soumen Ash and Moumita for the helpful assistance and suggestion. I would also like to thanks Dr. Bharat, Dr. Kasi, Dr. Arabinda, Dr. Gohil and Sandeep who have contributed to make my stay very pleasant with their healthy discussion and friendship nature.

Outside the academic field, I also want to thank my great buddy Amarpreet, Mantesh, Bijoy, Ashish, Vikas and Jitender who are my best friend at IIT Delhi and make my life fruitful and enjoyable. We had a great time together and we are always be the best friend.

Finally, my highest appreciation is addressed to my entire families especially my Mom and Dad for their blessings and support. Without their love and care the completion of this thesis would not have been possible. I also want to thank my brother, sister, my Bhabhi (sister-in-law) and nephew for their love and motivation.

I am heartily grateful to my wife Sukhi who enabled me to seamlessly continue my thesis. Huge thanks to my wife for her understanding, self-giving support, patient, inspiration, and endless love which helped me a lot to pursue my research. She always motivated and encouraged me in tough times, providing me courage to handle the situations when I am facing difficulties during my work. I want to express my eternal gratitude to my in-laws for providing their tremendous support, encouragement, indispensable understanding and who have always faith on my abilities to achieve my target.

I acknowledge the financial support of CSIR for a fellowship and IIT Delhi for providing me all research facilities. Lastly, I want to thank my dear God for granting me an opportunity and privilege to successfully pursue this assignment.

Soumen Saha

ABSTRACT

Growing concerns over the global warming and exhaustion of fossil fuels reserves have triggered an urgent demand for replace fossil fuels with clean and sustainable energy sources. To effectively address these issues renewable energy plays a very crucial contribution in the energy conversion processes. Electrochemical water splitting is the most convenient way to supply oxygen and hydrogen as water is abundant in nature. Molecular hydrogen has been considered as one of the most promising energy sources for replacing fossil fuels by renewable and sustainable energy sources. Oxygen evolution reaction is similarly important in fuel cells. Despite several efforts made for designing an active and durable electrocatalysts for the production of hydrogen/oxygen, it remains a significant challenge to find an electrocatalyst with similar or better activity than Pt for HER and Ir/Ru based materials for OER.

Here, we concentrated our study on the development of efficient and durable electrocatalysts based on low cost and earth-abundant transition metal alloys. The activity of these catalysts were affected by their composition. Composition has a crucial role in the enhancement of the activity of such alloys for either HER or OER. This thesis begins with an introduction which includes some fundamental properties and synthesis of nano materials using different techniques, and mainly the details of electrocatalytic (HER & OER) and magnetic studies. Finally we discuss the conclusions and future prospects of using of various alloys as advanced electrocatalysts.

Chapter 1 (Introduction) deals with literature survey on the importance of water splitting reaction for the production of hydrogen and oxygen including the mechanism. We have also described different methods (microemulsion and hydrothermal and co-precipitation) for synthesizing alloy

nanomaterials. Finally, we give a brief on the principles of different characterization techniques, magnetic properties and basic of electrochemical reaction (HER and OER).

In chapter 2, nanostructured copper-cobalt-nickel alloys of varied stoichiometry have been synthesized as an alternative to the costly Pt-based alloys using the reverse micellar method. Magnetic studies confirms the presence of super-paramagnetic order and saturation magnetization is enhanced with increasing cobalt to nickel ratio. Low onset overpotential with enhanced catalytic activity was observed for the CuCoNi (111) alloys.

Chapter 3 discusses the synthesis of Ni₃Co/G composites using a co-precipitation method followed by thermal reduction under hydrogen atmosphere for 5h. The Ni₃Co/G composites were investigated towards hydrogen evolution reaction (HER) as electrocatalysts in alkaline media (0.5 M KOH), which show an excellent electrocatalytic activity with an over-potential of 95 mV to reach 10 mA.cm² current density toward HER. The high activity of Ni₃Co/G is due to the synergistic effect and faster electron transfer between graphene and Ni₃Co alloy in Ni₃Co/G composite during electrochemical reaction.

In chapter 4, unsupported nickel-molybdenum alloy nanocatalysts were synthesized by a two-step hydrothermal-thermal reduction method. The electrochemical study shows that HER current density of the alloy increases with the increase in Mo content. The NiMo alloy catalyst shows good stability for 16 h under the given conditions.

In Chapter 5, ternary FeCoNi alloy nanocatalysts has been demonstrated as a superior catalyst for electrochemical oxygen evolution reaction in alkaline media. This ternary nanoalloy could be prepared from layered double hydroxides of FeCoNi, followed by thermal reduction at 700 °C under reducing atmosphere. Introduction of third element in binary alloy has a heavy influence on

the OER performances, and FeCoNi electrode has proved to have superior activity compared with the other two nanostructures FeNi and CoNi alloy.

In chapter 6, we discuss the characterization and electro-catalytic properties of iron-nickel alloy nanoparticles of varying stoichiometry. Face-centered cubic phase was observed for alloys rich in Ni (FeNi₃ and FeNi), however Fe₃Ni alloy nanoparticles are dominant with bcc structure mixed with a some percent of fcc phase of iron-nickel alloys when the iron is present in major amount.

Electrochemical analysis shows that FeNi₃ alloys exhibits higher performance for oxygen evolution reaction compared to other compositions of iron nickel alloys (FeNi and Fe₃Ni).

Conclusions and future prospects have been discussed in **Chapter 7**. Binary and ternary nanocatalysts have been fabricated and good control over composition was displayed. Synthesized alloy nanoparticles were tested electrochemically with respect to the benchmark parameter for HER and OER to assess their performance in strong alkaline/acidic condition. Finally, the thesis gives deep understanding about materials, processes, and methods which can be used to make efficient water splitting device from earth-abundant and low-cost materials.

सार

ग्लोबल वार्मिंग पर बढ़ते चिंता और जीवाश्म ईंधन भंडार के थकावट ने जीवाश्म ईंधन को स्वच्छ और टिकाऊ ऊर्जा स्रोतों के साथ बदलने की एक तत्काल मांग की है। इन मुद्दों को प्रभावी ढंग से संबोधित करने के लिए अक्षय ऊर्जा रूपांतरण प्रक्रियाओं में बहुत महत्वपूर्ण योगदान देती है। इलेक्ट्रोकेमिकल पानी बंटवारे ऑक्सीजन और हाइड्रोजन की आपूर्ति का सबसे सुविधाजनक तरीका है क्योंकि पानी प्रकृति में प्रचुर मात्रा में है। अक्षय हाइड्रोजन को अक्षय और टिकाऊ ऊर्जा स्रोतों द्वारा जीवाश्म ईंधन की जगह के लिए सबसे अधिक प्रचलित ऊर्जा स्रोतों में से एक माना जाता है। ऑक्सीजन विकास प्रतिक्रिया इसी तरह ईंधन कोशिकाओं में महत्वपूर्ण है। हाइड्रोजन/ऑक्सीजन के उत्पादन के लिए एक सक्रिय और टिकाऊ इलेक्ट्रोकेटिस्टिस्ट तैयार करने के कई प्रयासों के बावजूद, HER के लिए Pt और OER के लिए Ir/Ru आधारित सामग्रियों की तुलना में इसी तरह की या बेहतर गतिविधि के साथ एक इलेक्ट्रोकेटलिस्ट को खोजने के लिए यह एक महत्वपूर्ण चुनौती है।

यहां, हमने कम लागत और धरती-प्रचुर मात्रा में संक्रमण धातु मिश्र धातुओं के आधार पर कुशल और टिकाऊ इलेक्ट्रोकेटिस्टिस्ट के विकास पर हमारे अध्ययन पर ध्यान केंद्रित किया। इन उत्प्रेरक की गतिविधि उनकी रचना से प्रभावित थी इस तरह की गतिविधि को बढ़ाने के लिए HER और OER के लिए संरचना की महत्वपूर्ण भूमिका है। यह थीसिस एक परिचय के साथ शुरू होता है जिसमें विभिन्न मूलभूत तकनीकों का उपयोग करने वाले नैनो सामग्री के कुछ मौलिक गुण और संश्लेषण शामिल हैं, और मुख्य रूप से इलेक्ट्रोकेटिकल (HER और OER) और चुंबकीय अध्ययनों का विवरण। अंत में हम उन्नत इलेक्ट्रोकेटिस्टिस्ट के रूप में विभिन्न मिश्र धातुओं के उपयोग के निष्कर्ष और भविष्य की संभावनाओं पर चर्चा करते हैं।

अध्याय 1 (परिचय) तंत्र सहित हाइड्रोजन और ऑक्सीजन के उत्पादन के लिए पानी के बंटवारे की प्रतिक्रिया के महत्व पर साहित्य सर्वेक्षण से संबंधित है। हमने मिश्र धातुओं के नैनोमिटरियल्स के संश्लेषण के लिए विभिन्न तरीकों (सूक्ष्ममुद्रा और जलतापीय और सह-वर्षा) का भी वर्णन किया है। अंत में, हम विभिन्न लक्षण वर्णन तकनीकों, चुंबकीय गुणों और विद्युत रासायनिक प्रतिक्रिया (HER और OER) के मूल सिद्धांतों के बारे में संक्षिप्त जानकारी देते हैं।

अध्याय 2 में, विविध स्टोइकीओमेट्री के Copper-cobalt-nickel मिश्र धातुओं के नैनोस्ट्रक्चर्ड मिश्र धातुओं को रिवर्स माइक्रोनेलर विधि का इस्तेमाल करते हुए महंगा पीटी आधारित मिश्र धातु के विकल्प के रूप में संश्लेषित किया गया है। चुंबकीय अध्ययनों से सुपर-पैरामाग्नेटिक ऑर्डर की उपस्थिति की पुष्टि की जाती है और संतृप्ति चुंबकत्व निकल अनुपात कोबाल्ट में बढ़ रही है। Cu-Co-Ni (111) मिश्र धातुओं के लिए बढ़ाया उत्प्रेरक गतिविधि के साथ कम शुरुआत की अधिक संभावनाएं देखी गईं।

अध्याय 3 5h के लिए हाइड्रोजन वातावरण के तहत थर्मल में कमी के बाद एक सह-वर्षा विधि का उपयोग करते हुए Ni₃Co/G के संश्लेषण की चर्चा करता है। Ni₃Co/G कंपोजिटों की जांच की गई है जो हाइड्रोजन विकास प्रतिक्रिया (HER) के रूप में क्षारीय मीडिया (0.5 M) में इलेक्ट्रोकेटिस्टिस्ट के रूप में है, जो 95 mV की अधिक क्षमता वाले एक उत्कृष्ट इलेक्ट्रोकेटिकल गतिविधि को 10 mA.cm² तक पहुंचने के लिए

वर्तमान घनत्व को दर्शाती है। $\text{Ni}_3\text{Co}/\text{G}$ की उच्च गतिविधि विद्युत रासायनिक प्रतिक्रिया के दौरान $\text{Ni}_3\text{Co}/\text{G}$ कम्पोजिट में सपरगिस्टिक प्रभाव और graphene और Ni_3Co मिश्र धातु के बीच तेजी से इलेक्ट्रॉन हस्तांतरण की वजह से है।

अध्याय 4 में, बिना-समर्थित निकल-मोलिब्डेनम मिश्र धातु नैनोउत्प्रेरक को दो-चरण जल-तापीय-थर्मल घटाना विधि द्वारा संश्लेषित किया गया था। इलेक्ट्रोकेमिकल अध्ययन से पता चलता है कि Mo सामग्री में वृद्धि के साथ मिश्र धातु की वर्तमान घनत्व बढ़ जाती है। NiMo मिश्र धातु उत्प्रेरक दी गई स्थितियों के तहत 16 घंटे के लिए अच्छी स्थिरता दिखाता है।

अध्याय 5 में, टेर्नरी फेकोनी मिश्र धातु नैनोउत्प्रेरक को क्षारीय मीडिया में इलेक्ट्रोकेमिकल ऑक्सीजन विकास प्रतिक्रिया के लिए बेहतर उत्प्रेरक के रूप में दिखाया गया है। इस त्रिगुट नैनोलीय को FeCoNi के स्तरित डबल हाइड्रोक्साइड से तैयार किया जा सकता है, इसके बाद कम से कम $700\text{ }^\circ\text{C}$ में वातावरण कम करने के बाद तापीय कमी की जा सकती है। द्विआधारी मिश्र धातु में तीसरे तत्व का परिचय OER प्रदर्शन पर भारी प्रभाव पड़ता है, और FeCoNi इलेक्ट्रोड अन्य दो नैनोस्ट्रक्चर FeNi और CoNi मिश्र धातु के मुकाबले बेहतर गतिविधि साबित हुआ है।

अध्याय 6 में, हम लोहे-निकल मिश्र धातु नैनोकणों के अलग-अलग स्टेइचीमेट्री के लक्षण वर्णन और विद्युत-उत्प्रेरक गुणों पर चर्चा करते हैं। Ni (FeNi_3 and FeNi) में समृद्ध मिश्र धातुओं के लिए fcc चरण का निरीक्षण किया गया था, हालांकि लोहे की प्रमुख मात्रा में मौजूद लोहे-निकल मिश्र धातुओं के fcc चरण के कुछ प्रतिशत के साथ मिश्रित बीसीसी संरचना के साथ Fe_3Ni मिश्र धातु नैनोकणों प्रमुख हैं। इलेक्ट्रोकेमिकल विश्लेषण से पता चलता है कि FeNi_3 मिश्र धातुओं के निकल मिश्र धातुओं (FeNi and Fe_3Ni) की अन्य रचनाओं की तुलना में ऑक्सीजन विकास प्रतिक्रिया के लिए उच्च प्रदर्शन दर्शाती हैं।

अध्याय 7 में निष्कर्ष और भविष्य की संभावनाओं पर विचार विमर्श किया गया है। बाइनरी और त्रिगुट नैनोउत्प्रेरक का गढ़ा हुआ है और संरचना पर अच्छे नियंत्रण प्रदर्शित किए गए हैं। मजबूत क्षारीय/अम्लीय हालत में उनके प्रदर्शन का आकलन करने के लिए संश्लेषित मिश्र धातु नैनोकणों को HER और OER के लिए बेंचमार्क पैरामीटर के संबंध में विद्युतचुंबकीय तरीके से परीक्षण किया गया था। अंत में, थीसिस सामग्री, प्रक्रियाओं, और विधियों के बारे में गहरे समझ देता है जिनका उपयोग पृथ्वी से कुशल जल विभेदक उपकरण बनाने के लिए किया जा सकता है।

TABLE OF CONTENTS

CERTIFICATE	i
ACKNOWLEDGEMENTS	iii
ABSTRACT	v
LIST OF FIGURES	xv
LIST OF TABLES	xxii
ABBREVIATIONS	xxiii
CHAPTER 1: Introduction	
1.1 Energy and catalysis	3
1.2 Electrochemical water splitting reaction	5
1.3 Hydrogen evolution reaction (HER) mechanism	6
1.4 Oxygen evolution reaction (OER)	8
1.5 Electrocatalysis of alloy materials	9
1.6 Volcano plot	9
1.7 Different methodologies used for synthesis of nanomaterials	11
1.7.1 Hydrothermal Method	11
1.7.2 Reverse micellar method	13
1.7.3 Co-precipitation/refluxing method for LDHs preparation	16
1.8 Characterization Techniques	17
1.8.1 Powder X-ray Diffraction (PXRD)	17
1.8.2 Scanning electron microscope (SEM)/ Field Emission Electron Microscopy (FESEM):	18

1.8.3	Principles of TEM operation	21
1.8.4	X-ray photoelectron spectroscopy	22
1.9	Properties of materials	24
1.9.1	Magnetic properties	24
1.9.2	Electrocatalytic properties	27
1.9.2.1	Working electrode	27
1.9.2.2	Reference electrode	28
1.9.2.3	Counter electrode (Auxiliary electrode)	28
1.9.2.4	Cyclic voltammetry using a three electrode setup	29
1.9.2.5	Linear Sweep Voltammetry (LSV)	31
1.9.2.6	Chronoamperometric / Chronopotentiometric Analysis	32
1.9.2.7	Tafel slope	33
1.9.2.8	Electrochemical impedance spectroscopy (EIS)	34
1.10	References	36

CHAPTER 2: Copper-cobalt-nickel alloys: An efficient and durable electrocatalyst in acidic media

2.1	Abstract	45
2.2	Introduction	45
2.3	Materials and Methods	47
2.3.1	Materials	47
2.3.2	Preparation of the copper-cobalt-nickel alloy nano catalysts	48
2.4	Characterization techniques	48
2.4.1	Powder x-ray diffraction	48

2.4.2	Scanning electron microscopy	49
2.4.3	Transmission electron microscopy	49
2.4.4	Magnetic measurements	49
2.4.5	Electrochemical measurements	49
2.5	Results and discussion	51
2.5.1	Structure, morphology and elemental analysis	51
2.5.2	Magnetization study	56
2.5.3	Hydrogen evolution reaction study and analysis	57
2.5.4	Tafel plots and stability of the electrocatalyst	58
2.6	Conclusions	62
2.7	References	62

CHAPTER 3: Ni₃Co/G composite as an earth-abundant robust and stable electrocatalyst for hydrogen evolution reaction

3.1	Abstract	68
3.2	Introduction	68
3.3	Materials and Methods	71
3.3.1	Materials	71
3.3.2	Preparation of the Ni ₃ Co/G composite	71
3.4	Characterization techniques	72
3.4.1	Powder x-ray diffraction	72
3.4.2	Scanning electron microscopy	72
3.4.3	Transmission electron microscopy	72
3.4.4	Electrochemical measurements	72

3.5	Results and discussion	74
3.5.1	Structure, morphology and elemental analysis	74
3.5.2	Hydrogen evolution reaction	79
3.5.3	Electrochemical impedance spectroscopy	82
3.5.4	Tafel slope analysis	83
3.5.5	Stability of the electrocatalyst	83
3.6	Conclusions	86
3.7	References	87

CHAPTER 4: Hydrogen evolution reaction (HER) using nickel-molybdenum alloy electrocatalyst

4.1	Abstract	93
4.2	Introduction	93
4.3	Experimental	96
4.3.1	Materials	96
4.3.2	Synthesis of nickel-molybdenum alloys	96
4.4	Characterization techniques	97
4.4.1	Powder x-ray diffraction	97
4.4.2	Field emission scanning electron microscopy	97
4.4.3	Transmission electron microscopy	97
4.4.4	Electrochemical measurements	98
4.5	Results and discussion	98
4.5.1	Structure, morphology and elemental analysis	98
4.5.2	Hydrogen evolution reaction study and analysis	103

4.5.3	Tafel slope analysis	105
4.5.4	Stability of the electrocatalyst after HER study and analysis	107
4.6	Conclusions	109
4.7	References	110

CHAPTER 5: FeCoNi alloy as noble metal-free electrocatalyst for oxygen evolution reaction (OER)

5.1	Abstract	116
5.2	Introduction	116
5.3	Materials and Methods	119
5.3.1	Materials	119
5.3.2	Preparation of the FeCoNi alloy nano catalysts	119
5.3.3	Synthesis of FeNi and CoNi	120
5.4	Characterization techniques	120
5.4.1	Powder x-ray diffraction	120
5.4.2	Scanning electron microscopy	121
5.4.3	Transmission electron microscopy	121
5.4.4	XPS Measurements	121
5.4.5	Electrochemical measurements	122
5.5	Results and discussion	123
5.5.1	Structure, morphology and elemental analysis	123
5.5.2	XPS analysis	129
5.5.3	Oxygen evolution reaction studies and Tafel study	131

5.5.4	Electrochemical impedance spectroscopy	134
5.5.5	Stability of electrocatalyst after OER study	136
5.6	Conclusions	138
5.7	References	139

CHAPTER 6: Composition dependent electrocatalytic activity of iron-nickel alloys towards oxygen evolution reaction (OER)

6.1	Abstract	146
6.2	Introduction	146
6.3	Materials and Methods	149
6.3.1	Materials	149
6.3.2	Synthesis of iron-nickel alloy nano catalysts	149
6.4	Characterization techniques	149
6.4.1	Powder x-ray diffraction	149
6.4.2	Scanning electron microscopy	150
6.4.3	Transmission electron microscopy	150
6.4.4	X-ray Photoelectron Spectroscopy	150
6.4.5	Electrochemical measurements	150
6.5	Results and discussion	152
6.5.1	Structure, morphology and elemental analysis	152
6.5.2	XPS analysis	159
6.5.3	Oxygen evolution reaction	160
6.5.4	Impedance analysis	165
6.5.5	Stability of the electrocatalyst after OER	165

study and analysis

6.6 Conclusions 168

6.7 References 168

CHAPTER 7 Summary and future prospects 176

Bio-Data

LIST OF FIGURES

Figure 1.1. Hydrogen evolution reaction mechanism in acidic solutions on the surface of an electrode. -----	8
Figure 1.2. Volcano plot and ΔG_H values for the hydrogen evolution reaction (HER) for various pure metals and metal overlayers calculated at 1 bar of H ₂ (298 K). -----	10
Figure 1.3. Schematic diagram of autoclave equipment used in the hydrothermal synthesis. --	12
Figure 1.4. Schematic diagram of microemulsion showing the mechanism formation of nanoparticles through intermicellar exchange of droplets. -----	14
Figure 1.5. Schematic diagram of an x-ray tube that could be used for the production of x-ray. -----	18
Figure 1.6. Schematic diagram of scanning electron microscope (SEM). -----	20
Figure 1.7. A simplified ray diagram of a transmission electron microscope. -----	22
Figure 1.8. Schematic diagram showing the basic principle of XPS. -----	23
Figure 1.9. . Schematic showing adjacent magnetic dipole moments in (a) Paramagnetic, (b) Ferromagnetic, (c) Antiferromagnetic and (d) Ferrimagnetic material. -----	26
Figure 1.10. Three electrode system for electrochemical reaction. -----	29
Figure 1.11. Current response in a cyclic voltammetric study. -----	30
Figure 1.12. Tafel plot η vs. $\log i$. -----	34

Figure 2.1. Phase diagram of Cu-Co-Ni alloy	
Figure 2.2. Powder X-ray diffraction patterns of copper-cobalt-nickel alloy nanoparticles.	52
Figure 2.3. SEM images and x-ray elemental mapping of CuCoNi (1:1:1) alloy nanoparticles; (a) SEM image and elemental mapping of (b) copper(blue), (c) cobalt (red) and (d) nickel (green).	53
Figure 2.4. SEM-EDS patterns of CuCoNi (1:1:1), CuCoNi (1:2:1) and CuCoNi (1:1:2) alloy nanoparticles.	54
Figure 2.5. TEM micrographs of (a) CuCoNi (1:1:1) (b) CuCoNi (1:2:1) and (c) CuCoNi (1:1:2) alloy.	55
Figure 2.6. (a-b) HRTEM micrographs of CuCoNi (1:1:1) alloy nanostructures.	55
Figure 2.7. M vs. H plots of copper-cobalt-nickel alloy nanoparticles at 5 K.	56
Figure 2.8. (a) LSV polarization curves of the bare GC and CuCoNi (1:1:1)/GC, CuCoNi (1:2:1)/GC and CuCoNi (1:1:2)/GC in 0.5 M H ₂ SO ₄ solution at a scan rate of 5 mV s ⁻¹ . (b) Enlargement of the hatched region in (a).	57
Figure 2.9. Tafel plot of the copper-cobalt-nickel alloy catalyst.	59
Figure 2.10. The cycling stability of the CuCoNi (1:1:1)/GC electrode over 500 scanning cycles.	60

Figure 2.11. PXRD pattern of CuCoNi (1:1:1) alloy before and after 500 cycles of hydrogen evolution reaction. -----	60
Figure 2.12. TEM images of CuCoNi (1:1:1) alloy before and after 500 cycles of hydrogen evolution reaction. -----	61
Figure 2.13. LSV polarization curves of the CuCoNi(1:1:1)/GC electrode at the different scan numbers. -----	61
Figure 3.1. Schematic illustration for the preparation of Ni ₃ Co/G composite. -----	74
Figure 3.2. Powder X-ray diffraction patterns of Ni-hydroxide, Co-hydroxide and Ni ₃ Co/G hydroxide. -----	75
Figure 3.3. Powder X-ray diffraction patterns of Ni/Ni ₃ S ₂ , Co/Co ₉ S ₈ and Ni ₃ Co/G composite nanoparticles.-----	76
Figure 3.4. SEM images of (a)Ni-hydroxide,(b) Co-hydroxide, (c)rGO and Ni ₃ Co/G composite nanoparticles. -----	77
Figure 3.5. SEM-EDS mapping image of Ni ₃ Co/G composite nanoparticles and the corresponding elemental mapping of Ni(green), Co(red) and Carbon(sky-blue). -----	78
Figure 3.6. (a)TEM image, (b) magnified image of (a), (c) SAED pattern and (d) HRTEM image of Ni ₃ Co/G composite nanoparticles.-----	79
Figure 3.7. (a) LSV polarization curves of the Ni/Ni ₃ S ₂ , Co/Co ₉ S ₈ , Ni ₃ Co and Ni ₃ Co/G at a scan rate of 5 mV s ⁻¹ . (b) Enlargement of the shadow pattern in (a), (c) Comparison of charge-transfer resistances; Nyquist plots of Ni/Ni ₃ S ₂ , Co/Co ₉ S ₈ , Ni ₃ Co and Ni ₃ Co/G electrodes and (d)	

corresponding Tafel plot of the Ni/Ni ₃ S ₂ , Co/Co ₉ S ₈ , Ni ₃ Co and Ni ₃ Co/G alloys in 0.5 M KOH solution.-----	80
Figure 3.8. (a) Continual electrolysis for 16 h at the fixed overpotential to produce a current density of 10 mA.cm ⁻² ; (b) Polarization curves for Ni ₃ Co/G composite obtained before (black line) and after (red line) 16h chronopotentiometric study. -----	84
Figure 3.9. PXRD pattern of Ni ₃ Co/G composite before and after 16 h of chronopotentiometric study for hydrogen evolution reaction.-----	85
Figure 3.10. (a) SEM mapping images and (b) EDS composition of Ni ₃ Co/G composite nanoparticles after 16 h of chronopotentiometric study for hydrogen evolution reaction.-----	85
Figure 3.11. TEM mapping images of Ni ₃ Co/G composite nanoparticles before (a) and after (b) 16 h of chronopotentiometric study for hydrogen evolution reaction.-----	86
Figure 4.1. Schematic illustration for the preparation of nickel-molybdenum alloys.-----	99
Figure 4.2. Powder X-ray diffraction patterns of (a) NiMoO ₄ .xH ₂ O and (b) NiMo and Ni ₂ Mo alloy nanoparticles.-----	100
Figure 4.3. FESEM patterns of (a-c) Ni ₂ Mo and (d-f) NiMo alloy nanoparticles.-----	101
Figure 4.4. SEM-EDS mapping images of NiMo (a-c) and corresponding EDS data (d).-----	102
Figure 4.5. SEM-EDS mapping images of Ni ₂ Mo (a-c) and corresponding EDS data (d). ----	102
Figure 4.6. TEM patterns of (a) Ni ₂ Mo and (b) NiMo alloy nanoparticles.-----	103
Figure 4.7. (a) LSV polarization curves of the bare GCE, Ni, Ni ₂ Mo and NiMo in 0.5 M H ₂ SO ₄ solution at a scan rate of 5 mV s ⁻¹ . (b) Enlargement of the shadow pattern in (a). -----	104

Figure 4.8. Tafel plot of the bare GCE, Ni, Ni ₂ Mo and NiMo in 0.5 M H ₂ SO ₄ solution. -----	106
Figure 4.9. (a) Continual electrolysis for 16 h at a current density of 10 mA.cm ⁻² ; (b) Stability of the NiMo alloy modified on GCE electrode initial LSV polarization(black line) and the one after (green line) 16h chronopotentiometric study. -----	107
Figure 4.10. (a) PXRD pattern of NiMo alloy before and after 16h of chronopotentiometric study for hydrogen evolution reaction. -----	108
Figure 4.11. (a) TEM images of NiMo alloy (a) before and (b) after 16h of chronopotentiometric study for hydrogen evolution reaction. -----	109
Figure 5.1. Powder X-ray diffraction patterns of FeNi, CoNi and FeCoNi alloy nanoparticles.-----	123
Figure 5.2. SEM images of (a) FeNi, (b) FeCoNi and (c) CoNi alloy nanoparticles. -----	124
Figure 5.3. SEM-EDS mapping image of FeCoNi alloy nanoparticles and the corresponding elemental mapping of Fe(magenta), Ni(green) and Co(pink) . -----	125
Figure 5.4. SEM-EDS mapping image of CoNi alloy nanoparticles and the corresponding elemental mapping of Ni(green) and Co(red).-----	126
Figure 5.5. SEM-EDS mapping image of FeNi alloy nanoparticles and the corresponding elemental mapping of Ni(green) and Fe(magenta).-----	127
Figure 5.6. TEM images of (a) FeNi, (b) FeCoNi and (c) CoNi alloy nanoparticles. -----	128
Figure 5.7. (a) TEM image (b) the magnified HRTEM image and (c) SAED pattern of alloy of FeCoNi alloy nanoparticles. -----	129

Figure 5.8. XPS spectrum of FeCoNi. XPS survey (a) and high resolution spectra of Fe2p (b) Ni2p (c) and Co 2p (d). -----	130
Figure 5.9. (a) LSV polarization curves of the bare Pt and FeNi, CoNi and FeCoNi in 0.5 M KOH solution at a scan rate of 5 mV s ⁻¹ . (b) Enlargement of the shadow pattern in (a), (c) corresponding Tafel plot of the FeNi, CoNi and FeCoNi catalyst and (d) LSV polarization curves of the FeCoNi electrode at three different consecutive scan number.-----	132
Figure 5.10. Comparison of charge-transfer resistances; Nyquist plots of FeNi, CoNi and FeCoNi electrodes in 0.5 M KOH solution.-----	134
Figure 5.11. (a) Continual electrolysis for 10 h at the fixed overpotential to produce a current density of 10 mA.cm ⁻² ; (b) Stability of the FeCoNi alloy modified on Pt electrode initial LSV polarization(solid line) and the one after (dashed line) 10h chronopotentiometric study.-----	137
Figure 5.12. (a) PXRD pattern and (b) SEM-EDX mapping image of FeCoNi alloy before and after 10h of chronopotentiometric study for oxygen evolution reaction. -----	138
Figure 6.1. Powder X-ray diffraction patterns of FeNi ₃ , FeNi and Fe ₃ Ni alloy nanoparticles.-----	153
Figure 6.2. SEM image of (a) FeNi, (b) FeNi ₃ and (c) Fe ₃ Ni hydroxide. -----	154
Figure 6.3. SEM image of (a) FeNi, (b) FeNi ₃ and (c) Fe ₃ Ni alloy nanoparticles. -----	154
Figure 6.4. SEM-EDS (a-d) mapping image of FeNi ₃ nanoparticles and the corresponding elemental mapping of Fe (red) and Ni (green). -----	155

Figure 6.5. SEM-EDS mapping image of FeNi alloy nanoparticles and the corresponding elemental mapping of Fe(red) and Ni(green). -----	156
Figure 6.6. SEM-EDS mapping image of Fe ₃ Ni alloy nanoparticles and the corresponding elemental mapping of Fe(red) and Ni(green). -----	157
Figure 6.7. (a)TEM image, (b) Enlargement of the TEM image (a), (c) the magnified HRTEM image and (d) SAED pattern of alloy of FeNi ₃ alloy nanoparticles. -----	158
Figure 6.8. TEM images of (a) Fe ₃ Ni and (b) FeNi alloy nanoparticles. -----	159
Figure 6.9. XPS of (a) Ni 2p and (b) Fe 2p in FeNi ₃ alloy nanoparticles. -----	160
Figure 6.10. (a) LSV polarization curves of the bare Pt and FeNi ₃ , FeNi and Fe ₃ Ni in 0.5 M KOH solution at a scan rate of 5 mV s ⁻¹ . (b) Enlargement of the shadow pattern in (a), (c) corresponding Tafel plot and (d) Nyquist plots of the alloy electrodes using 0.5 M KOH solution.-----	162
Figure 6.11. (a) Continual electrolysis for 10 h at a fixed current density of 10 mA.cm ⁻² ; (b) Stability of the FeNi ₃ alloy modified on Pt electrode initial LSV polarization(solid line) and the one after 10h chronopotentiometric study (dashed line). -----	166
Figure 6.12. (a) PXRD pattern and (b-e) SEM-EDS mapping image of FeNi ₃ alloy before and after 10h of chrono study for hydrogen evolution reaction. -----	167

LIST OF TABLES

Table 2.1. The EDS analysis of copper-cobalt-nickel alloy nanoparticles (error: 3-5%).-----	53
Table 3.1. Comparison of HER performances of Ni ₃ Co/G composite with other non-noble-metal electrocatalyst in alkaline media. -----	81
Table 5.1. Elemental analysis result for a FeCoNi alloy. -----	126
Table 5.2. Elemental analysis result for a CoNi alloy. -----	127
Table 5.3. Elemental analysis result for a FeNi alloy. -----	128
Table 5.4: Comparison of OER activities in alkaline media for FeCoNi ternary alloy with other non-noble metal OER electrocatalyst.-----	135
Table 6.1. Comparison of OER activity in alkaline media for iron-nickel nanoparticles with other non-noble metal OER electrocatalyst.-----	163

ABBREVIATIONS

Å	Angstroms
cm	Centimeter
nm	Nanometer
T	Temperature
o	Degree
2θ	Two Theta
λ	Wavelength
T _N	Neel Temperature
T _c	Curie Temperature
K	Kelvin
Ω	Ohm
eV	Electron volt
NPs	Nanoparticles
CTAB	Cetyltrimethylammonium bromide
XRD	X-ray Diffraction
PXRD	Powder X-ray Diffraction
SDBS	Sodium dodecylbenzenesulfonate
SEM	Scanning Electron Microscopy
FESEM	Field Emission Scanning Electron Microscopy
TEM	Transmission Electron Microscopy
HRTEM	High Resolution Transmission Electron Microscopy

ED	Electron diffraction
EDS	Energy Dispersive Spectroscopy
EDX	Energy-dispersive X-ray spectroscopy
XPS	X-ray Photoelectron Spectroscopy
CV	Cyclic Voltammetry
LSV	Linear Sweep Voltammetry
ECSA	Electrochemically Active Surface Area
EIS	Electrochemical Impedance Spectroscopy
HER	Hydrogen Evolution Reaction
OER	Oxygen Evolution Reaction
RE	Reference Electrode
R_{ct}	Charge Transfer Resistance
GCE	Glassy Carbon Electrode
C_{dl}	Double Layer Capacitance
WE	Working Electrode
CE	Counter Electrode
RHE	Reversible Hydrogen Electrode
μ	Magnetic Moment
H	Magnetic Field
M	Magnetization
rGO	Reduced graphene oxide
G	Graphene
χ_m	Molar Magnetic Susceptibility

Ms	Saturation Magnetization
emu	Electromagnetic Unit
vs.	Versus
J/I	Current Density
H	Applied Field
eq.	Equation
°C	Centigrade
μm	Micrometer
mm	Millimetres
min	Minutes
h	Hours
s	Seconds